


Thermal crossover, transition, and coexistence in Fermi polaronic spectroscopiesHiroyuki Tajima¹ and Shun Uchino²¹*Quantum Hadron Physics Laboratory, RIKEN Nishina Center (RNC), Wako, Saitama 351-0198, Japan*²*Waseda Institute for Advanced Study, Waseda University, Shinjuku, Tokyo 169-8050, Japan* (Received 14 December 2018; revised manuscript received 12 February 2019; published 12 June 2019)

We investigate the thermal evolution of radio-frequency (RF) spectra of a spin-imbalanced Fermi gas near a Feshbach resonance in which degenerate Fermi-polaron and classical Boltzmann-gas regimes emerge in the low-temperature and high-temperature limits, respectively. By using self-consistent frameworks of strong-coupling diagrammatic approaches, both the ejection and the reserve RF spectra available in cold-atom experiments are analyzed. We find a variety of transfers from Fermi polarons to the Boltzmann gas such that a thermal crossover expected in the weak-coupling regime is shifted to a sharp transition near unitarity and to double-peak coexistence of attractive and repulsive branches in the strong-coupling regime. Our theory provides semiquantitative descriptions for a recent experiment on the ejection RF spectroscopy at unitarity [Z. Yan, P. B. Patel, B. Mukherjee, R. J. Fletcher, J. Struck, and M. W. Zwierlein, *Phys. Rev. Lett.* **122**, 093401 (2019)] and suggests the importance of beyond-two-body correlations in the high-temperature regime due to the absence of Pauli-blocking effects.

DOI: [10.1103/PhysRevA.99.063606](https://doi.org/10.1103/PhysRevA.99.063606)**I. INTRODUCTION**

A spectroscopic method is one of the central themes in physics including hadron-mass spectroscopy in nuclear physics [1–3] and gravitational wave detection in astrophysics [4,5]. In condensed matter, a spectroscopic technique is of importance to examine low-energy excitations in many-body systems, which has led to discoveries of pseudogaps in high- T_c superconductors [6–8] and of topological states of matter [9]. In an ultracold atomic gas that is an ideal platform to realize nontrivial quantum states of matter and yet has limited probes due to electrical charge neutrality, a many-body spectroscopy is an inevitable tool to extract fundamental properties of the system [10]. For instance, Bragg spectroscopy allows one to measure Nambu-Goldstone modes in superfluid gases [11,12], and lattice modulation spectroscopy allows one to measure the Mott gap in an optical lattice system [13]. In addition, radio-frequency (RF) spectroscopy in cold atoms has revealed essential properties such as the pseudogap [14–17], the superfluid gap [18], the Higgs mode [19], and the Efimov effect [20,21]. Since the RF spectroscopy is sensitive to excitation properties in quantum many-body systems, of current interest in RF spectrum measurements is a polaron which is a prototype of how a strong interaction affects quasiparticle properties.

In cold atoms, polarons can be achieved by a polarized mixture. When such a mixture consists of a two-component Fermi gas, the system at a low-temperature reduces to a Fermi polaron, which is a mobile impurity surrounded by the Fermi sea. The RF spectral results as well as the experimental realizations [22–27] have triggered a number of theoretical works mostly under the condition of a single impurity at absolute zero [28–48]. The current consensus is that such single-impurity calculations agree well with low-temperature spectral data of experiments at typical impurity concentrations.

Quite recently, the MIT group tracked the thermal evolution of the RF spectra of a spin-imbalanced unitary Fermi

gas in a homogeneous box potential [49] from the low-temperature quantum regime to the classical Boltzmann-gas regime [50]. The observed temperature dependence of the RF spectra indicates the existence of a nontrivial sharp transition between quantum and classical regimes, in addition to a precise determination of the polaron energy. Obviously, an explanation of the MIT experiment demands self-consistent theoretical frameworks to take the strong correlations into account [51–59].

In this article, motivated by the MIT experiment [50], we investigate the thermal evolution of RF spectra of a strongly interacting polarized Fermi gas by means of self-consistent many-body calculations. By analyzing typical schemes of the RF spectroscopy, we demonstrate that a transfer from Fermi polarons to Boltzmann gas becomes rich due to correlation effects. In particular, we find three types of transfers such as crossover, transition, and coexistence as a function of the interaction strength, as schematically depicted in Fig. 1. A comparison with the experiment at unitarity shows that our calculations perfectly reproduce the spectral properties in a low-temperature regime and yet have some deviations in a high-temperature regime, implying the importance of beyond-two-body scattering processes due to the absence of Pauli-blocking effects of majority fermions.

II. FORMALISM

We consider a spin-imbalanced Fermi gas with a large scattering length a such that $|k_F a| > 1$, where k_F is the Fermi momentum. (In what follows, we use $\hbar = k_B = 1$ and the system volume is taken to be unity.) In RF spectroscopy, an RF field is applied to an atomic cloud, which introduces a transition between one of the spin states and another atomic excited state, and the current of the excited state induced by the transition is measured [10]. Since the position of a Feshbach resonance is different between different internal states, one can realize a couple of schemes of RF spectroscopy. In

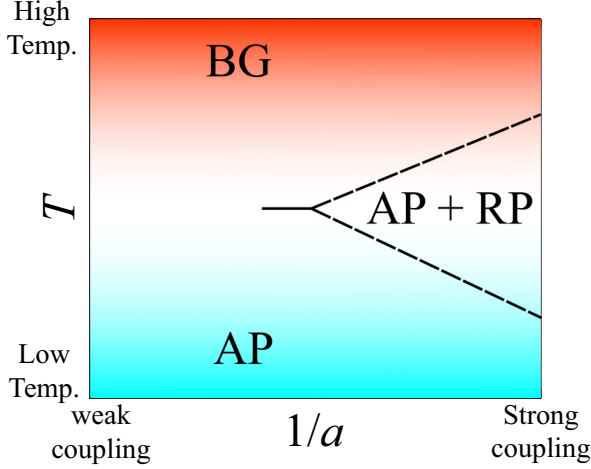


FIG. 1. Schematic diagram for polarized Fermi gases at a finite temperature near unitarity obtained from ejection RF spectra, where AP (BG) is the regime of attractive polarons (Boltzmann gas). Solid and dashed lines show the transition and the boundary for the coexistence regime (AP + RP), respectively.

ejection RF spectroscopy, a strongly interacting atomic gas is initially prepared and is transferred to a weakly interacting final state. By neglecting the final-state interaction effect and assuming a small Rabi frequency, Ω_R , to justify the linear response treatment, the RF spectrum as a function of the energy ω is given by [10,50]

$$I_E(\omega) = 2\pi\Omega_R^2 \sum_{\mathbf{p}} f(\xi_{\mathbf{p},\downarrow} - \omega) A_{\mathbf{p},\downarrow}(\xi_{\mathbf{p},\downarrow} - \omega). \quad (1)$$

Here, $f(\xi) = (e^{\xi/T} + 1)^{-1}$ is the Fermi distribution function, $A_{\mathbf{p},\sigma}(\omega)$ the spectral function, T the temperature, and $\xi_{\mathbf{p},\sigma} = \frac{p^2}{2m} - \mu_\sigma$ the kinetic energy of a Fermi atom measured from the chemical potential μ_σ with momentum \mathbf{p} , mass m , and pseudospin $\sigma = \uparrow, \downarrow$, where \uparrow (\downarrow) corresponds to the majority (minority) component. In reverse RF spectroscopy, in contrast, a weakly interacting atomic gas is initially prepared and is transferred to a strongly interacting final state. In this case, the spectrum in the absence of the initial-state interaction is given by [10,27]

$$I_R(\omega) = 2\pi\Omega_R^2 \sum_{\mathbf{p}} f(\xi_{\mathbf{p},\uparrow}) A_{\mathbf{p},\downarrow}(\xi_{\mathbf{p},\downarrow} + \omega), \quad (2)$$

where $\sigma = i$ in Eq. (2) indicates the initial state of reverse RF measurements. The spectral function $A_{\mathbf{p},\sigma}(\omega) = -\frac{1}{\pi} \text{Im} G_{\mathbf{p},\sigma}(i\omega_n \rightarrow \omega + i\delta)$ is obtained from the analytic continuation of thermal Green's function $G_{\mathbf{p},\sigma}(i\omega_n) = [i\omega_n - \xi_{\mathbf{p},\sigma} - \Sigma_{\mathbf{p},\sigma}(i\omega_n)]^{-1}$, where ω_n and $\Sigma_{\mathbf{p},\sigma}(i\omega_n)$ are the fermionic Matsubara frequency and the self-energy, respectively [60]. We use a Padé approximation with a small number $\delta = 10^{-2}\varepsilon_F$ for the analytic continuation (ε_F is the Fermi energy of the majority atoms) [56]. We note that μ_σ is determined by solving an equation for the number density $n_\sigma = T \sum_{\mathbf{p},\omega_n} G_{\mathbf{p},\sigma}(i\omega_n)$. According to the MIT experiment [50], the impurity concentration $x = \frac{n_\downarrow}{n_\uparrow}$ is fixed as $x = 0.1$. The many-body correlations associated with the strong interaction are included in the self-energy. In this article, we employ

the extended T -matrix approximation (ETMA) [56,61–65], which can reproduce observed ground-state properties in both imbalanced [56] and balanced [66,67] Fermi gases near the unitarity limit. In this formalism, $\Sigma_{\mathbf{p},\sigma}(i\omega_n)$ is given by

$$\Sigma_{\mathbf{p},\sigma}(i\omega_n) = T \sum_{\mathbf{q},\nu_j} \Gamma_{\mathbf{q}}(i\nu_j) G_{\mathbf{q}-\mathbf{p},-\sigma}(i\nu_j - i\omega_n), \quad (3)$$

where

$$\Gamma_{\mathbf{q}}(i\nu_j) = \left[\frac{m}{4\pi a} + \Pi_{\mathbf{q}}(i\nu_j) - \sum_{\mathbf{p}} \frac{m}{p^2} \right]^{-1} \quad (4)$$

is the many-body T -matrix with the scattering length a and ν_j is the bosonic Matsubara frequency. The pair susceptibility $\Pi_{\mathbf{q}}(i\nu_j)$ is given by

$$\Pi_{\mathbf{q}}(i\nu_j) = T \sum_{\mathbf{p},\omega_n} G_{\mathbf{p}+\mathbf{q},\uparrow}^0(i\omega_n + i\nu_j) G_{-\mathbf{p},\downarrow}^0(-i\omega_n), \quad (5)$$

where $G_{\mathbf{p},\sigma}^0(i\omega_n) = (i\omega_n - \xi_{\mathbf{p},\sigma})^{-1}$ is the bare Green's function.

III. RESULTS

Figure 2 shows the ejection RF spectra $I_E(\omega)$ and the reverse RF spectra $I_R(\omega)$ at different temperatures for $(k_F a)^{-1} = 0$ and $(k_F a)^{-1} = 0.4$, respectively, and the line

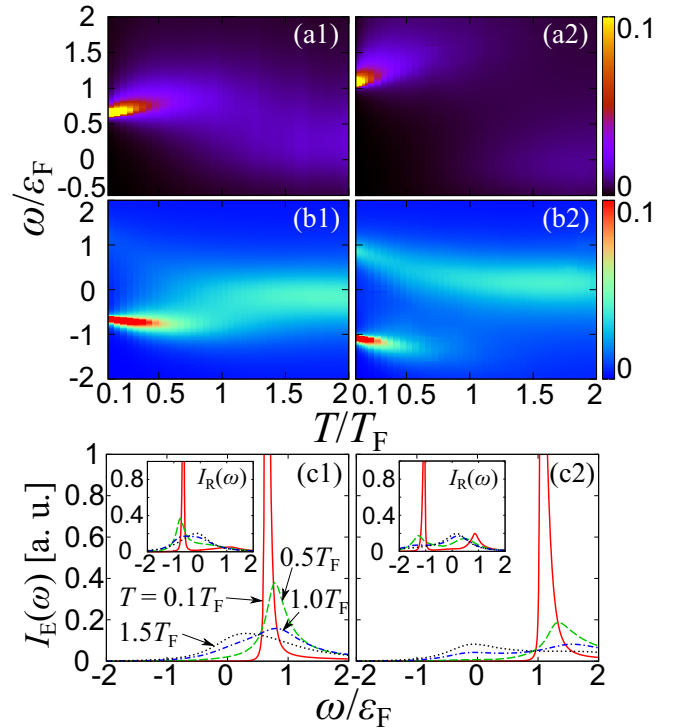


FIG. 2. Calculated ejection RF spectra $I_E(\omega)$ [panels (a1) and (a2)] and reverse RF spectra $I_R(\omega)$ [panels (b1) and (b2)] in arbitrary units. Panels (c1) and (c2) show the line shapes of $I_E(\omega)$ [the inset is $I_R(\omega)$]. The interactions are set at $(k_F a)^{-1} = 0$ [panels (a1), (b1), and (c1)] and $(k_F a)^{-1} = 0.4$ [panels (a2), (b2), and (c2)]. ε_F and T_F are the Fermi energy and the Fermi temperature of the majority atoms, respectively. The common line styles are used in each figure.

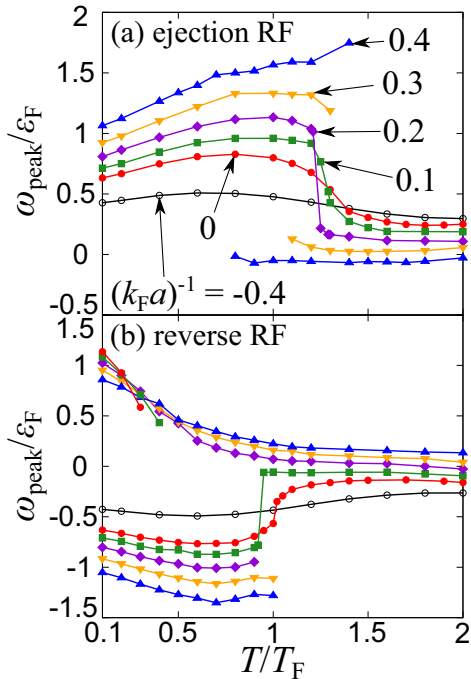


FIG. 3. Peak positions ω_{peak} of (a) ejection and (b) reverse RF spectra at different interaction strengths. The common line symbols are used in each figure.

shapes of $I_E(\omega)$ and $I_R(\omega)$ are reported in Fig. 2. In accordance with the different ω dependencies, it follows that each RF spectrum shows different features associated with the properties of the system. The ejection RF spectra reveal the occupied state at the thermal equilibrium since impurities in the thermodynamic many-body state are transferred to the weakly interacting final state. At a low temperature, $I_E(\omega)$ has a strong intensity near the attractive branch given by $-E_a$, where $E_a < 0$ is the attractive polaron energy. Such a peak is shifted towards the low-energy regime associated with a Boltzmann gas or repulsive branch with increasing the temperature. We note that the peak energy slightly increases with increasing the temperature at $T \lesssim 0.8T_F$ reflecting the increase of $|E_a|$. In contrast, excitation properties of impurities are probed by the reverse RF spectrum in which the weak-interacting initial state is transferred to the strongly interacting minority state. In this regard, one can see the second peak near the repulsive branch associated with the repulsive polaron energy $E_r > 0$ in addition to the attractive branch around $\omega = E_a$. To see how the thermal evolution of the spectra is affected by the repulsive branch, in Fig. 3, we plot the peak positions ω_{peak} of (a) ejection and (b) reverse RF spectra at different impurity-bath interaction strengths. At the weak coupling $(k_F a)^{-1} = -0.4$ where the repulsive branch is absent, regardless of the schemes of the RF spectroscopy, we see the smooth crossover from attractive polarons at the low-temperature regime to the Boltzmann gas in the high-temperature regime. By increasing the interaction, the crossover behavior becomes gradually sharper around $T/T_F = 1$ and changes to the transitionlike jump at $(k_F a)^{-1} \simeq 0.1$. In the ejection RF spectra, the single curve present in the weak-coupling regime is split into the two curves at $(k_F a)^{-1} \simeq 0.3$, and the temperature region where the

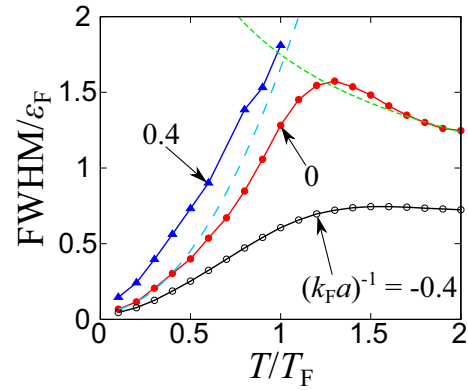


FIG. 4. FWHM of the ejection RF spectra at different interaction strengths. The dashed (long-dashed) line represents the high (low)-temperature fitting $\gamma/\varepsilon_F = 1.75\sqrt{T_F/T}$ [$\gamma/\varepsilon_F = 1.61(T/T_F)^2$] at $(k_F a)^{-1} = 0$ [50,68–71].

double peaks coexist emerges. In contrast, we find different behaviors between the ejection and reverse RF spectroscopies due to the existence of the repulsive branch. In particular, the result for $I_E(\omega)$ at $(k_F a)^{-1} = 0.4$ shows that the lower peak associated with the repulsive branch appears around $T/T_F \simeq 0.8$ and the upper peak associated with the attractive branch disappears around $T/T_F \simeq 1.4$, since it is largely broadened and overlaps with the lower peak. In contrast to the ejection RF, we find the coexistence of two peaks in the low-temperature region of the reverse RF spectra. This is because the peak of the repulsive branch evolves even at a low temperature as increasing the interaction. In addition, as the temperature increases, the repulsive peak corresponding to E_r decreases due to the competition between the self-energy shift on the repulsive branch and the thermal agitation. We note that this behavior is in sharp contrast to the behavior of the repulsive polaron energy as a function of the impurity concentration [56]. Moreover, the peak of the attractive branch disappears around $T/T_F = 1$ beyond $(k_F a)^{-1} \simeq 0.2$. This indicates that the transition to the Boltzmann gas is deeply related to the existence of the repulsive polaron in the strong-coupling regime. In the high-temperature limit, both RF spectra converge to the single peak.

In Fig. 4, we show the full width at half maximum (FWHM) of the ejection RF spectra, which is directly related to the decay rate of quasiparticles. At the weak coupling $(k_F a)^{-1} = -0.4$ and unitarity, the FWHM has a maximum in the intermediate-temperature region. In particular, the result at unitarity in the high-temperature regime is well fitted by the classical Boltzmann limit $\gamma/\varepsilon_F = 1.75\sqrt{T_F/T}$ [50,68–71]. Thus, attractive polarons in fact undergo the Boltzmann gas regime beyond the maximum of the FWHM. While the repulsive polaron is expected to undergo such a classical regime at the strong coupling $(k_F a)^{-1} = 0.4$, the FWHM is ill-defined because two broad peaks overlap each other [see Fig. 2(c2)]. On the other hand, we find the increase of the FWHM in the low-temperature regime as increasing the temperature at each interaction strength. This growth gets stronger with increasing the interaction due to the collisional decoherence effects of attractive polarons at a finite impurity concentration [27]. The

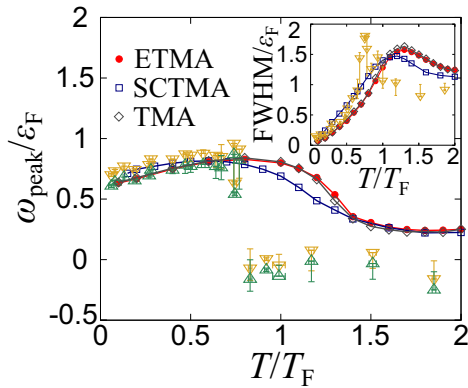


FIG. 5. Comparisons of peak positions and FWHM (inset) in ejection RF spectra between our results (solid circle, ETMA; open square, SCTMA; open diamond, TMA) and recent experiments at the unitarity limit. The downward and upward triangles represent the experimental value from Ref. [50] and that with the subtraction of the mean-field shift with respect to the final state interaction given by $\Sigma_f = 0.09\epsilon_F$, respectively.

quadratic behavior of the decay rate $\gamma/\epsilon_F = 1.61(T/T_F)^2$ [69] is obtained at unitarity, which is consistent with the Fermi-liquid theory [70]. We now compare our formalism with the recent experiment at unitarity [50]. To this end, in addition to the ETMA, we perform two different diagrammatic approximations; the non-self-consistent [51–53] and self-consistent T -matrix approximations [65,72–74], which are abbreviated as TMA and SCTMA, respectively. In Fig. 5, we show the comparisons of peak positions and the FWHM values in the ejection RF spectra. We note that while the TMA self-energy is obtained by replacing G with G^0 in Eq. (3), SCTMA is the approximation such that two G^0 in Eq. (5) are replaced by G . It is notable that our results for the spectral peak quantitatively reproduce the experiment (with the subtraction of the mean-field shift of the final-state interaction) up to $T/T_F \simeq 0.75$, where the sharp transition between attractive polarons and Boltzmann gas occurs. While our results are consistent with the second-order virial expansion [59], we find the discrepancy between our results and the experiment around the transition temperature. In addition, the fitting coefficients of the decay rate in both high-temperature and low-temperature regimes deviate from the experimental values quantitatively. In the low-temperature regime, the deviation of the FWHM occurs in the TMA and the ETMA, which can be explained by a collisional decay process associated with dressed particles at finite impurity concentration as discussed in the context of the polaron-to-polaron decay process of the repulsive polaron [27,75]. While the TMA and the ETMA do not include such a process, the SCTMA does it through the dressed propagators in the pair susceptibility, Eq. (5). Indeed, the quadratic fit of the SCTMA gives $\gamma/\epsilon_F = 2.95(T/T_F)^2$, which is close to the experimental result [$\gamma/\epsilon_F = 2.71(T/T_F)^2$] [50]. We note that the SCTMA also shows an excellent agreement with the experiments near the superfluid critical temperature in balanced Fermi gases [65,68,73,76–78].

In contrast, the discrepancy in the high-temperature regime is related to multibody correlations, which may be considered

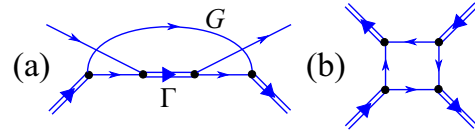


FIG. 6. Feynman diagrams describing examples of (a) three-body and (b) four-body correlations which are absent in the TMA, where the solid (double-solid) lines represent G (Γ). While the ETMA involves three-body correlations (a), the SCTMA involves both three-body (a) and four-body (b) correlations.

to be negligible in two-component Fermi gases due to the Pauli-blocking effect. When the Fermi surface is thermally depleted, however, the Pauli-blocking effect is suppressed. Therefore, beyond-two-body correlations can have a significant effect on the Fermi polarons at finite temperature as in the case of a Bose polaron [79–88]. Since the experiment can be well reproduced by our theories in the low-temperature regime, where the Pauli-blocking effect emerges, we argue that beyond-two-body correlations, such as three-body scattering, shift the critical interaction for the sharp transition towards the weaker coupling regime. Furthermore, we uncover the difference among three different diagrammatic approaches in terms of three- and four-body correlations. While the TMA involves an atom-dimer scattering process within the Born level, the ETMA and the SCTMA include the second-order three-body correlations as shown in Fig. 6(a). In addition, SCTMA includes the lowest-order four-body correlations shown in Fig. 6(b), which are absent in both the TMA and the ETMA. Indeed, the SCTMA is closest to the experiment around $T/T_F = 1$ among these approaches. Although our formalism does not fully explain the experiment, we find that the results are sensitive to the different approximations in the intermediate-temperature region, implying the importance of multibody correlations. Our finding is consistent with the result of the virial expansion [59,71].

IV. CONCLUSION

In conclusion, we have investigated the thermal evolution of radio-frequency spectra in an imbalanced Fermi gas system from the quantum degenerate state to the classical Boltzmann regime using the many-body T -matrix approximation. We have predicted that the thermal evolution is classified into three types: smooth crossover, sharp transition, and double-peak coexistence, where the recent experiment at MIT has detected the second one at the unitarity limit. These three types are transferred to each other by shifting the impurity-bath interaction. They can be detected in future experiments with finite scattering lengths. We have also revealed that the repulsive polarons play significant roles in the thermal evolution of the RF spectra. From the quantitative viewpoint, our results perfectly reproduce the observed peak position of ejection RF spectra up to $T/T_F \simeq 0.75$ but deviate from it in the high-temperature regime where the Pauli-blocking is absent. To explain the high-temperature regime, our results strongly suggest the necessity of a self-consistent formalism beyond the existing approximations that contains multibody correlations.

ACKNOWLEDGMENTS

We thank Z. Yan and M. W. Zwierlein for providing us with their experimental data for comparison. H.T. thanks F. Scazza, M. Zaccanti, D. Kagamihara, and R. Sato for useful discus-

sions. H.T. is supported by a Grant-in-Aid for JSPS fellows (Grant No. 17J03975). S.U. is supported by JSPS KAKENHI Grant No. JP17K14366 and by a Waseda University Grant for Special Research Projects (Grant No. 2018S-209). This work was partially supported by the RIKEN iTHEMS program.

- [1] Y. Nakahara, M. Asakawa, and T. Hatsuda, *Phys. Rev. D* **60**, 091503(R) (1999).
- [2] M. Asakawa, T. Hatsuda, and Y. Nakahara, *Prog. Part. Nucl. Phys.* **46**, 459 (2001).
- [3] E. Klempt and J.-M. Richard, *Rev. Mod. Phys.* **82**, 1095 (2010).
- [4] B. P. Abbott *et al.* (LIGO Scientific Collaboration and Virgo Collaboration), *Phys. Rev. Lett.* **119**, 161101 (2017).
- [5] B. P. Abbott *et al.* (SKA South Africa/MeerKAT), *Astrophys. J.* **848**, L12 (2017).
- [6] C. Renner, B. Revaz, J.-Y. Genoud, K. Kadowaki, and Ø. Fischer, *Phys. Rev. Lett.* **80**, 149 (1998).
- [7] A. Damascelli, Z. Hussain, and Z.-X. Shen, *Rev. Mod. Phys.* **75**, 473 (2003).
- [8] Ø. Fischer, M. Kugler, I. Maggio-Aprile, C. Berthod, and C. Renner, *Rev. Mod. Phys.* **79**, 353 (2007).
- [9] D. Lu, I. N. Vishik, M. Yi, Y. Chen, R. G. Moore, and Z.-X. Shen, *Annu. Rev. Condens. Matter Phys.* **3**, 129 (2012).
- [10] P. Törmä, Spectroscopies—Theory, in *Quantum Gas Experiments: Exploring Many-Body States*, edited by P. Törmä and K. Sengstock (Imperial College, London, 2015).
- [11] J. Steinhauer, R. Ozeri, N. Katz, and N. Davidson, *Phys. Rev. Lett.* **88**, 120407 (2002).
- [12] S. Hoinka, P. Dyke, M. G. Lingham, J. J. Kinnunen, G. M. Bruun, and C. J. Vale, *Nat. Phys.* **13**, 943 (2017).
- [13] T. Stoferle, H. Moritz, C. Schori, M. Kohl, and T. Esslinger, *Phys. Rev. Lett.* **92**, 130403 (2004).
- [14] C. Chin, M. Bartenstein, A. Altmeyer, S. Riedl, S. Jochim, J. Hecker Denschlag, and R. Grimm, *Science* **305**, 1128 (2004).
- [15] J. T. Stewart, J. P. Gaebler, and D. S. Jin, *Nature (London)* **454**, 744 (2008).
- [16] J. P. Gaebler, J. T. Stewart, T. E. Drake, D. S. Jin, A. Perali, P. Pieri, and G. C. Strinati, *Nat. Phys.* **6**, 569 (2010).
- [17] Y. Sagi, T. E. Drake, R. Paudel, R. Chapurin, and D. S. Jin, *Phys. Rev. Lett.* **114**, 075301 (2015).
- [18] A. Schirotzek, Y.-I. Shin, C. H. Schunk, and W. Ketterle, *Phys. Rev. Lett.* **101**, 140403 (2008).
- [19] A. Behrle, T. Harrison, J. Kombe, K. Gao, M. Link, J.-S. Bernier, C. Kollath, and M. Köhl, *Nat. Phys.* **14**, 781 (2018).
- [20] T. Lompe, T. B. Ottenstein, F. Serwane, A. N. Wenz, G. Zürn, and S. Jochim, *Science* **330**, 940 (2010).
- [21] S. Nakajima, M. Horikoshi, T. Mukaiyama, P. Naidon, and M. Ueda, *Phys. Rev. Lett.* **106**, 143201 (2011).
- [22] A. Schirotzek, C.-H. Wu, A. Sommer, and M. W. Zwierlein, *Phys. Rev. Lett.* **102**, 230402 (2009).
- [23] S. Nascimbène, N. Navon, K. J. Jiang, L. Tarruell, M. Teichmann, J. McKeever, F. Chevy, and C. Salomon, *Phys. Rev. Lett.* **103**, 170402 (2009).
- [24] C. Kohstall, M. Zaccanti, M. Jag, A. Trenkwalder, P. Massignan, G. M. Bruun, F. Schreck, and R. Grimm, *Nature (London)* **485**, 615 (2011).
- [25] M. Koschorreck, D. Pertot, E. Vogt, B. Fröhlich, M. Feld, and M. Köhl, *Nature (London)* **485**, 619 (2012).
- [26] M. Cetina, M. Jag, R. S. Lous, I. Fritsche, J. T. M. Walraven, R. Grimm, J. Levinsen, M. M. Parish, R. Schmidt, M. Knap, and E. Demler, *Science* **354**, 96 (2016).
- [27] F. Scazza, G. Valtolina, P. Massignan, A. Recati, A. Amico, A. Burchianti, C. Fort, M. Inguscio, M. Zaccanti, and G. Roati, *Phys. Rev. Lett.* **118**, 083602 (2017).
- [28] P. Massignan, M. Zaccanti, and G. M. Bruun, *Rep. Prog. Phys.* **77**, 034401 (2014).
- [29] R. Combescot and S. Giraud, *Phys. Rev. Lett.* **101**, 050404 (2008).
- [30] G. M. Bruun and P. Massignan, *Phys. Rev. Lett.* **105**, 020403 (2010).
- [31] R. Schmidt, T. Enss, V. Pietilä, and E. Demler, *Phys. Rev. A* **85**, 021602(R) (2012).
- [32] J. E. Baarsma, J. Armaitis, R. A. Duine, and H. T. C. Stoof, *Phys. Rev. A* **85**, 033631 (2012).
- [33] F. Chevy, *Phys. Rev. A* **74**, 063628 (2006).
- [34] R. Combescot, A. Recati, C. Lobo, and F. Chevy, *Phys. Rev. Lett.* **98**, 180402 (2007).
- [35] M. Punk, P. T. Dumitrescu, and W. Zwerger, *Phys. Rev. A* **80**, 053605 (2009).
- [36] C. Mora and F. Chevy, *Phys. Rev. A* **80**, 033607 (2009).
- [37] X. Cui and H. Zhai, *Phys. Rev. A* **81**, 041602(R) (2010).
- [38] C. J. M. Mathy, M. M. Parish, and D. A. Huse, *Phys. Rev. Lett.* **106**, 166404 (2011).
- [39] C. Trefzger and Y. Castin, *Phys. Rev. A* **85**, 053612 (2012).
- [40] N. Prokof'ev and B. Svistunov, *Phys. Rev. B* **77**, 020408(R) (2008).
- [41] N. V. Prokof'ev and B. V. Svistunov, *Phys. Rev. B* **77**, 125101 (2008).
- [42] J. Vlietinck, J. Ryckebusch, and K. Van Houcke, *Phys. Rev. B* **87**, 115133 (2013).
- [43] P. Kroiss and L. Pollet, *Phys. Rev. B* **91**, 144507 (2015).
- [44] O. Goulko, A. S. Mishchenko, N. Prokof'ev, and B. Svistunov, *Phys. Rev. A* **94**, 051605(R) (2016).
- [45] R. Schmidt and T. Enss, *Phys. Rev. A* **83**, 063620 (2011).
- [46] K. Kamikado, T. Kanazawa, and S. Uchino, *Phys. Rev. A* **95**, 013612 (2017).
- [47] A. Bulgac, J. E. Drut, and P. Magierski, *Phys. Rev. A* **78**, 023625 (2008).
- [48] O. Goulko and M. Wingate, *Phys. Rev. A* **82**, 053621 (2010).
- [49] B. Mukherjee, Z. Yan, P. B. Patel, Z. Hadzibabic, T. Yefsah, J. Struck, and M. W. Zwierlein, *Phys. Rev. Lett.* **118**, 123401 (2017).
- [50] Z. Yan, P. B. Patel, B. Mukherjee, R. J. Fletcher, J. Struck, and M. W. Zwierlein, *Phys. Rev. Lett.* **122**, 093401 (2019).
- [51] P. Massignan, G. M. Bruun, and H. T. C. Stoof, *Phys. Rev. A* **77**, 031601(R) (2008).

- [52] P. Massignan, G. M. Bruun, and H. T. C. Stoof, *Phys. Rev. A* **78**, 031602(R) (2008).
- [53] V. Pietilä, *Phys. Rev. A* **86**, 023608 (2012).
- [54] E. V. H. Doggen and J. J. Kinnunen, *Phys. Rev. Lett.* **111**, 025302 (2013).
- [55] H. Hu, B. C. Mulkerin, J. Wang, and X.-J. Liu, *Phys. Rev. A* **98**, 013626 (2018).
- [56] H. Tajima and S. Uchino, *New J. Phys.* **20**, 073048 (2018).
- [57] W. E. Liu, J. Levinsen, and M. M. Parish, *Phys. Rev. Lett.* **122**, 205301 (2019).
- [58] S. I. Mistakidis, G. C. Katsimiga, G. M. Koutentakis, and P. Schmelcher, *New J. Phys.* **21**, 043032 (2019).
- [59] B. C. Mulkerin, X.-J. Liu, and H. Hu, [arXiv:1808.07671](https://arxiv.org/abs/1808.07671).
- [60] To obtain a precise contact parameter from the high-frequency line shape as done in Ref. [50], we require the Matsubara Green's function up to the very large number of the Matsubara frequency in our theoretical framework.
- [61] T. Kashimura, R. Watanabe, and Y. Ohashi, *Phys. Rev. A* **86**, 043622 (2012).
- [62] H. Tajima, T. Kashimura, R. Hanai, R. Watanabe, and Y. Ohashi, *Phys. Rev. A* **89**, 033617 (2014).
- [63] H. Tajima, R. Hanai, and Y. Ohashi, *Phys. Rev. A* **93**, 013610 (2016).
- [64] H. Tajima, R. Hanai, and Y. Ohashi, *Phys. Rev. A* **96**, 033614 (2017).
- [65] M. Pini, P. Pieri, and G. C. Strinati, *Phys. Rev. B* **99**, 094502 (2019).
- [66] H. Tajima, P. van Wyk, R. Hanai, D. Kagamihara, D. Inotani, M. Horikoshi, and Y. Ohashi, *Phys. Rev. A* **95**, 043625 (2017).
- [67] M. Horikoshi, M. Koashi, H. Tajima, Y. Ohashi, and M. Kuwata-Gonokami, *Phys. Rev. X* **7**, 041004 (2017).
- [68] T. Enss, R. Haussman, and W. Zwerger, *Ann. Phys. (N.Y.)* **326**, 770 (2011).
- [69] There is an offset $\simeq 0.05$ associated with δ used for the analytic continuation as well as the finite-impurity-density effect.
- [70] G. M. Bruun, A. Recati, C. J. Pethick, H. Smith, and S. Stringari, *Phys. Rev. Lett.* **100**, 240406 (2008).
- [71] M. Sun and X. Leyronas, *Phys. Rev. A* **92**, 053611 (2015).
- [72] R. Haussmann, W. Rantner, S. Cerrito, and W. Zwerger, *Phys. Rev. A* **75**, 023610 (2007).
- [73] R. Haussmann, M. Punk, and W. Zwerger, *Phys. Rev. A* **80**, 063612 (2009).
- [74] B. Frank, J. Lang, and W. Zwerger, *J. Exp. Theor. Phys.* **127**, 812 (2018).
- [75] P. Massignan and G. M. Bruun, *Eur. Phys. J. D* **65**, 83 (2011).
- [76] R. Rossi, T. Ohgoe, E. Kozik, N. Prokof'ev, B. Svistunov, K. Van Houcke, and F. Werner, *Phys. Rev. Lett.* **121**, 130406 (2018).
- [77] C. Carcy, S. Hoinka, M. G. Lingham, P. Dyke, C. C. N. Kuhn, H. Hu, and C. J. Vale, *Phys. Rev. Lett.* **122**, 203401 (2019).
- [78] B. Mukherjee, P. B. Patel, Z. Yan, R. J. Fletcher, J. Struck, and M. W. Zwierlein, *Phys. Rev. Lett.* **122**, 203402 (2019).
- [79] M.-G. Hu, M. J. Van de Graaff, D. Kedar, J. P. Corson, E. A. Cornell, and D. S. Jin, *Phys. Rev. Lett.* **117**, 055301 (2016).
- [80] Z. Z. Yan, Y. Ni, C. Robens, and M. W. Zwierlein, [arXiv:1904.02685](https://arxiv.org/abs/1904.02685).
- [81] N. B. Jørgensen, L. Wacker, K. T. Skalmstang, M. M. Parish, J. Levinsen, R. S. Christensen, G. M. Bruun, and J. J. Arlt, *Phys. Rev. Lett.* **117**, 055302 (2016).
- [82] M. Sun, H. Zhai, and X. Cui, *Phys. Rev. Lett.* **119**, 013401 (2017).
- [83] E. Nakano, H. Yabu, and K. Iida, *Phys. Rev. A* **95**, 023626 (2017).
- [84] P. Naidon, *J. Phys. Soc. Jpn.* **87**, 043002 (2018).
- [85] S. M. Yoshida, S. Endo, J. Levinsen, and M. M. Parish, *Phys. Rev. X* **8**, 011024 (2018).
- [86] D. Blume, *Phys. Rev. A* **99**, 013613 (2019).
- [87] K. Watanabe, E. Nakano, and H. Yabu, *Phys. Rev. A* **99**, 033624 (2019).
- [88] J. Takahashi, R. Imai, E. Nakano, and K. Iida, [arXiv:1904.08799](https://arxiv.org/abs/1904.08799).